# NATURAL CONVECTION ON CORRUGATED PLATES: A NUMERICAL CASE STUDY ABOUT MESHES, BOUNDARY CONDITIONS AND PHYSICAL DOMAIN DETERMINATION

**S. A. Verdério Júnior[a],**

**V. L. Scalon[b],**

**S. R. Oliveira[c],**

**P. J. Martins Coelho[d],**

Instituto Federal de Educação, Ciência e Tecnologia de São Paulo (IFSP)
Department of Industry
CEP 14804-296, Araraquara, SP, Brazil
[a]silvioverderio@ifsp.edu.br

Universidade Estadual Paulista "Júlio de Mesquita Filho" (UNESP)
Faculdade de Engenharia de Bauru (FEB)
Department of Mechanical Engineering
CEP 17033-360, Bauru, SP, Brazil
[b]vicente.scalon@unesp.br
[c]santiago.oliveira@unesp.br

Instituto Superior Técnico (IST)
Universidade de Lisboa
Department of Mechanical Engineering
Av. Rovisco Pais 1, 1049-001 Lisboa, Portugal
[d]pedro.coelho@tecnico.ulisboa.pt

## ABSTRACT

The transfer of heat and mass by natural convection is present in the most diverse physical and chemical phenomena of nature and engineering equipment. In the last decades, the number of research on natural convection has grown dramatically, highlighting studies in physical-mathematical modeling and numerical solutions, experimental analysis and design and optimization techniques for fluid-thermal systems. This case study analyzed the influence of several numerical parameters in physical-mathematical modeling and numerical solution of natural convection heat transfer problems on isothermal plates with square waves in turbulent conditions of high Rayleigh number. The numerical parameters analyzed were the mesh refinement degree, wall boundary conditions (with or without wall functions implemented in the turbulent parameters) and computational physical domain influence. Free and open-source computational numerical tools were exclusively used in the construction of this work. Meshes with wall functions implemented in turbulent parameters presented greater accuracy and required less computational effort and simulation time, besides enabling the use of a lower degree of mesh refinement. The best numerical configuration of the physical model for the situation problem studied were defined from the criteria of accuracy, computational effort demanded, and stability and numerical convergence of the solution.

**Keywords:** heat transfer; natural convection; numerical analysis; corrugated plate; OpenFOAM®.

## NOMENCLATURE

| | |
|---|---|
| $C$ | empirical constant |
| $\hat{C}_p$ | heat capacity at constant pressure, J/(kg.K) |
| $C_{\varepsilon 1}$ | empirical constant of $\kappa - \varepsilon$ model |
| $C_{\varepsilon 2}$ | empirical constant of $\kappa - \varepsilon$ model |
| $C_\mu$ | empirical constant of $\kappa - \varepsilon$ model |
| $g$ | gravity acceleration, m/s² |
| $H_D$ | physical domain height, m |
| $k_t$ | thermal conductivity, W/(m. K) |
| $L_D$ | physical domain square base length, m |
| $L_P$ | plate longitudinal length, m |
| $n$ | empirical coefficient |
| $\overline{Nu}$ | average Nusselt number |
| $p$ | relative total pressure, m²/s² |
| $p\_rgh$ | relative dynamic pseudo-pressure, m²/s² |
| $p_0$ | relative incompressible total pressure, m²/s² |
| $Pr$ | Prandtl number |
| $Pr_t$ | turbulent Prandtl number |
| $\bar{P}$ | average relative pressure in the RANS model, Pa |
| $P_{atm}$ | atmospheric pressure, Pa |
| $P_\infty$ | free-stream pressure, Pa |
| $\overline{q''}$ | average convective heat flux over the plate, W/m² |
| $\overline{q''}_{REF}$ | reference average convective heat flux over the plate, W/m² |
| $Ra$ | Rayleigh number |
| $Ra_{L_P}$ | Rayleigh number, with plate longitudinal length as characteristic length |
| $S$ | mean absolute percentage deviation |
| $T$ | temperature field OpenFOAM® parameter, K |
| $\overline{T}_{REF}$ | average reference temperature, K |
| $\bar{T}$ | average component of temperature in the RANS model, K |
| $T_\infty$ | free-stream temperature, K |
| $T^+$ | non-dimensional temperature |
| $\overline{u_i}, \overline{u_j}$ | indicial velocity average components in the RANS model, m/s |
| $u^+$ | non-dimensional velocity |
| $U$ | velocity field OpenFOAM® parameter, m/s |
| $x_i, x_j$ | indicial coordinates, m |
| $z$ | elevation, m |

### Greek symbols

| | |
|---|---|
| $\alpha_t$ | turbulent thermal diffusivity, m²/s |
| $\beta$ | thermal coefficient of volume expansion, $K^{-1}$ |
| $\varepsilon$ | dissipation rate of turbulent kinetic energy, $m^2/s^3$ |

$\kappa$ turbulent kinetic energy, m²/s²
$\mu$ dynamic viscosity, kg/(m.s)
$\mu_t$ turbulence dynamic viscosity, kg/(m.s)
$\nu$ kinematic viscosity, m²/s
$\nu_t$ turbulence kinematic viscosity, m²/s
$\rho$ fluid density, kg/m³
$\bar{\rho}$ fluid density evaluated in $\bar{T}$, kg/m³
$\sigma_\varepsilon$ empirical constant of $\kappa - \varepsilon$ model
$\sigma_\kappa$ empirical constant of $\kappa - \varepsilon$ model
$\nabla$ gradient operator

## INTRODUCTION

Natural convection heat transfer problems, in laminar and turbulent regimes and the most diverse geometries, are increasingly receiving attention in the various branches of science and engineering. The demand for safer, more reliable, cheaper and more efficient cooling systems has grown significantly in the last decade, especially with technological development and the constant evolution of electrical and electronic systems and components – which are increasingly smaller, more integrated with each other and with greater density of power and heat generation. In this sense, cooling systems exclusively by natural convection – or complementary to conventional cooling systems by forced convection – are alternatives of great interest to the industry, which increasingly motivates research and investments in this area.

Fishenden e Saunders (1965), in one of the oldest and most important experimental references on the study of natural convection, proposed the famous empirical correlation of the type $\overline{Nu} = C.Ra^n$. Since then, the studies, research and applications of natural convection have grown significantly over the years.

In the last decade, the number of publications related to applications of natural convection – especially in the areas of physical-mathematical modeling, numerical and computational tools, experimental methodologies and project techniques for the optimization and design of robust thermal systems – has grown considerably. These publications are represented by studies of: Kitamura *et al.* (2015) in the experimental study of natural convection (laminar and turbulent) on horizontal flat plates and obtaining empirical correlations of the type $\overline{Nu}$ x $Ra$; Verdério Júnior *et al.* (2021a) and Verdério Júnior *et al.* (2021b) in the analysis of the main numerical parameters of influence and the creation and experimental validation of a numerical methodology for the study of natural convection (turbulent and laminar) in isothermal flat plates; Silva *et al.* (2021) in the numerical study of two different types of meshes (in different refinement degrees) applied to problems of turbulent natural convection on isothermal rectangular flat plates, with validation from experimental results; Gonçalves *et al.* (2021) in the applied experimental study of the Leidenfrost phenomenon in machining and analysis of the main parameters of influence; Verdério Júnior *et al.* (2021c) in obtaining a dimensionless formulation of the transport equations and the $\kappa - \varepsilon$ and $\kappa - \omega$ SST turbulence models for the study of turbulent natural convection; and Verdério Júnior *et al.* (2021d) in the formulation of an experimental methodology for the study of natural convection on flat and corrugated plates.

The present work is an extension of the analytical, numerical and experimental studies of the heat transfer process by natural convection on plates; which were made by Verdério Júnior *et al.* (2021a), Verdério Júnior *et al.* (2021b), Verdério Júnior *et al.* (2021c), Verdério Júnior *et al.* (2021d), and Silva *et al.* (2021)). Unlike the cited references that focus on the study of flat plates, this article directs its numerical analysis to corrugated plate geometries (with regular square waves) and in physical conditions of high Rayleigh number.

This case study aims to study the influence of the main numerical parameters in the physical-mathematical modeling and numerical solution of turbulent natural convection heat transfer problems on isothermal plates with regular square waves and in conditions of high Rayleigh number. The parameters studied were the mesh refinement degree, wall boundary conditions (with or without wall functions implemented in the turbulent parameters), and the computational physical domain.

Lastly, another objective of this work is to define the most adequate numerical configuration for the physical model of the problem situation studied. Another differential of this study is the exclusive use of free and open-source computational numerical tools.

## PROBLEM FORMULATION

### Geometry construction

The problem situation studied in this work is the turbulent natural convection on a plate with square waves and allocated in a large unbounded physical domain. The plate is assumed to be isothermal at 40°C, and the physical domain is initially filled with air at $T_\infty = 20$°C.

The plate has dimensions of 1 x 1 m and is composed of ten (10) square waves, with height and length equal to 0.05 m and equally spaced with each other with a span of 0.05 m. This plate geometry is located in the central region of a large independent open physical domain – with initial dimensions of 1.5 x 1.5 x 2.5 m, but whose final dimensions will be determined through physical domain definition tests. Figure 1 schematically illustrates the geometry of the total physical computational domain of the problem situation studied.

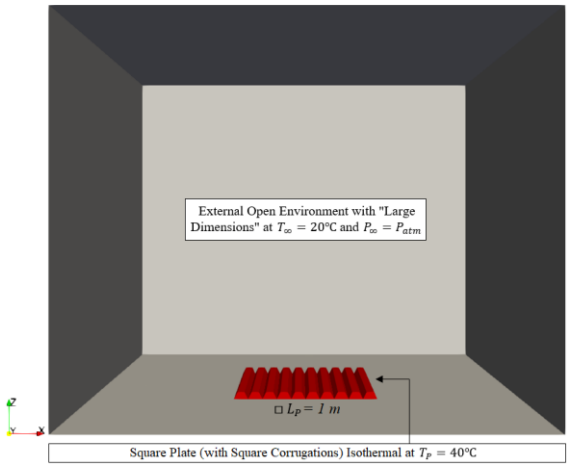


Figure 1. Total physical computational domain.

Adopting the origin of the coordinate system as the center of the corrugated plate and using the numerical strategy of double symmetry on the y and z axes, there are the definition of a reduced physical computational domain; as illustrated in Figure 2. To define and implement the boundary conditions, the new physical domain was subdivided into three regions: *free surfaces (*open external boundaries of the physical domain), *symmetry* (symmetry planes – left and front) and *plate (*solid wall region).

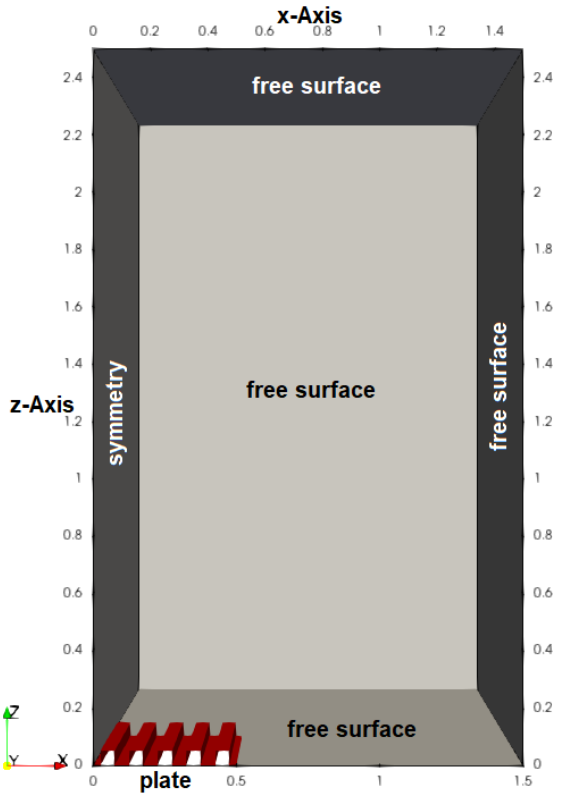


Figure 2. Reduced physical computational domain.

The free software SALOME, version 9.6.0, generated the CAD model in Figure 2. The different meshes used in this work were constructed from this CAD model and through the library cfMesh, version 1.1.

## Mesh definitions

The meshes used in this work are of the three-dimensional Cartesian hexahedral type, built with three (03) refinement zones. The levels of refinement decrease in a staggered manner from the plate region.

The $maxCellSize$ parameter of the cfMesh library – which controls the maximum edge size of the elements of a mesh, according to Juretic (2015) – was used in the definition of the different degrees of refinements and the construction of the seven (07) different mesh topologies used; as shown in Table 1. Figure 3 illustrates the less refined (with $maxCellSize = 1.50$) and more refined (with $maxCellSize = 0.70$) mesh settings used.

Table 1. Mesh topology used.

| *maxCellSize* | Elements | *maxCellSize* | Elements |
|---|---|---|---|
| 1.50 | 227902 | 0.90 | 917535 |
| 1.30 | 339299 | 0.80 | 1268869 |
| 1.15 | 475997 | | |
| 1.00 | 686060 | 0.70 | 1854078 |

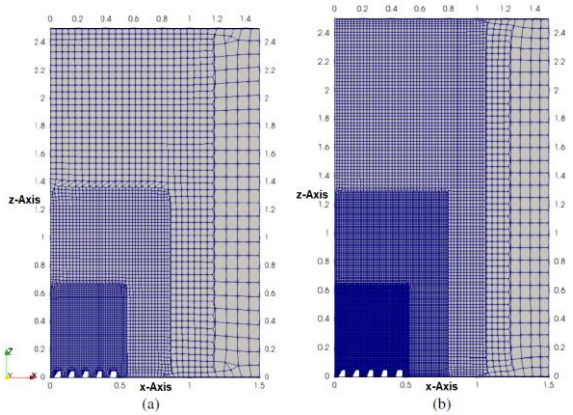


Figure 3. Meshes used: (a) less refined and (b) more refined.

## Mathematical and Numerical Model

Several simplifying hypotheses and physical and numerical models were adopted in modeling, and numerical solution of the physical-mathematical-numerical model governing the situation problem studied. Based on what is established in the references of Pope (2000), Bird *et al.* (2002), Vieser *et al.* (2002), Menter *et al.* (2003), Versteeg and Malalasekera (2007), Incropera *et al.* (2008), Çengel and Ghajar (2012), Bejan (2013), Çengel and Cimbala (2015), and Fox et al. (2018):

- The thermophysical properties of air are assumed constant and evaluated at $\bar{T}_{REF} = 303.15\ K$: $\nu = 1.6207 \cdot 10^{-5} m^2/s$, $\bar{\rho} = 1.1509\ kg/m^3$, $\hat{C}_p =$

$1007.1260\ J/(kg \cdot K)$, $\beta = 0.00323\ K^{-1}$, $Pr = 0.7066$, $Pr_t = 0.85$, and $k_t = 26.5331 \cdot 10^{-3}\ W/(m \cdot K)$.

- Air behaves like a Newtonian fluid, and Boussinesq's approximation is used to model and include buoyancy forces as a source term. So that:

$$\rho(\bar{T}) \approx \bar{\rho}[1 - \beta(\bar{T} - T_\infty)] \quad (1)$$

From the hypothesis of air as an ideal gas: $\beta = 1/\bar{T}_{REF}$.

- The effects of thermal radiation are inexpressive to the global energy balance and can be disregarded.
- The dimensions of the external physical domain are large enough not to exert a wall influence on the flow in free natural convection.
- Steady-state turbulent airflow with high Rayleigh number, equal to $Ra_{L_P} = 1.741.10^9$.
- Modeling and resolution through the RANS Method.
- The pressure-velocity-temperature coupling of the transport equations occurs through the SIMPLE algorithm, according to studies by Verdério Júnior (2015).
- Mass conservation equation in turbulent regime:

$$\frac{\partial \bar{u}_i}{\partial x_i} = 0 \quad (2)$$

- Application of Boussinesq's turbulent viscosity hypothesis to define the Momentum equations in turbulent regime:

$$\bar{\rho}\bar{u}_j \frac{\partial \bar{u}_i}{\partial x_j} = \frac{\partial}{\partial x_j}\left[(\mu + \mu_t)\left(\frac{\partial \bar{u}_i}{\partial x_j} + \frac{\partial \bar{u}_j}{\partial x_i}\right)\right] - \frac{\partial\left(\bar{P} + \frac{2}{3}\bar{\rho}\kappa + \bar{\rho}|g|z\right)}{\partial x_i} - \bar{\rho} g_i \beta(\bar{T} - T_\infty) \quad (3)$$

- Energy equation in turbulent regime:

$$\frac{\partial}{\partial x_j}\left(\bar{\rho}\bar{u}_j\bar{T}\right) = \frac{\partial}{\partial x_j}\left[\left(\frac{\mu}{Pr} + \frac{\mu_t}{Pr_t}\right)\frac{\partial \bar{T}}{\partial x_j}\right] \quad (4)$$

- $\kappa - \varepsilon$ turbulence model:

$$\nu_t = \frac{\mu_t}{\bar{\rho}} = C_\mu \frac{\kappa^2}{\varepsilon} \quad (5)$$

$$\bar{u}_j \frac{\partial \kappa}{\partial x_j} = \frac{\partial}{\partial x_j}\left[\left(\nu + \frac{\nu_t}{\sigma_\kappa}\right)\frac{\partial \kappa}{\partial x_j}\right] + \nu_t\left(\frac{\partial \bar{u}_i}{\partial x_j} + \frac{\partial \bar{u}_j}{\partial x_i}\right)\frac{\partial \bar{u}_i}{\partial x_j} - \varepsilon \quad (6)$$

$$\bar{u}_j \frac{\partial \varepsilon}{\partial x_j} = \frac{\partial}{\partial x_j}\left[\left(\nu + \frac{\nu_t}{\sigma_\varepsilon}\right)\frac{\partial \varepsilon}{\partial x_j}\right] + C_{\varepsilon 1}\frac{\varepsilon}{\kappa}\nu_t\left(\frac{\partial \bar{u}_i}{\partial x_j} + \frac{\partial \bar{u}_j}{\partial x_i}\right)\frac{\partial \bar{u}_i}{\partial x_j} - C_{\varepsilon 2}\frac{\varepsilon^2}{\kappa} \quad (7)$$

The empirical constants commonly used in this turbulence model are $C_{\varepsilon 1} = 1.44$, $C_{\varepsilon 2} = 1.92$, $C_\mu = 0.09$, $\sigma_\kappa = 1.0$, and $\sigma_\varepsilon = 1.3$.

- The influence of the buoyancy source terms in the modeling of production and/or destruction of $\kappa$ and $\varepsilon$ in the transport equations (6) and (7) is admitted to be negligible for this study.
- The Finite Volume Method (FVM) is used to solve discretized transport equations, implemented in OpenFOAM® software, version 2012.
- Transient numerical simulation, with scheduled termination for the convergence of the solution to the steady-state or until the 5000 iteration limit is reached.
- The other numerical aspects of the resulting physical-mathematical-numerical model: a) control and simulation execution parameters; b) numerical methods of discretization and interpolation of the transport equations terms; and c) methods, tolerances and control algorithms for solving the algebraic linear equations (obtained from the discretization of the transport equations) – are presented in detail and are the same used in Verdério Júnior *et al.* (2021a) and Verdério Júnior *et al.* (2021b).

**Boundary Conditions**

From the physical-numerical characteristics of the situation-problem studied, the solver *buoyantBoussinesqSimpleFoam* of OpenFOAM® was defined for the modeling, numerical structuring and solution.

From the division of the reduced physical domain of Figure 2 and the physical conditions of each region, there is the definition of boundary conditions for the following solver parameters: temperature, velocity, relative total pressure ($p = \bar{P}/\bar{\rho}$), relative dynamic pseudo pressure ($p\_rgh = p - |g|.z$), turbulent thermal diffusivity, turbulent kinetic energy, dissipation rate of turbulent kinetic energy, and turbulence kinematic viscosity.

Tables 2 and 3 illustrate the boundary conditions implemented in OpenFOAM® in the different regions of the physical domain, according to references by Moukalled *et al.* (2015) and OpenCFD (2020). The use of these boundary conditions was validated from experimental results in the references Verdério Júnior *et al.* (2021a) and Verdério Júnior *et al.* (2021b), in applications in the numerical study of natural convection on flat plates (in turbulent and laminar regimes).

Table 2. Boundary conditions of the regions of symmetry and free surface.

| Parameter | symmetry | free surfaces |
|---|---|---|
| $T\ [K]$ | Symmetry Condition | inletOutlet |
| $U\ [m/s]$ | | pressureInlet OutletVelocity |

| | | |
|---|---|---|
| $p\ [m^2/s^2]$ | | calculated |
| $p\_rgh$ $[m^2/s^2]$ | | totalPressure |
| $\alpha_t\ [m^2/s]$ | | $\nabla\alpha_t = 0$ |
| $\kappa\ [m^2/s^2]$ | | $\nabla\kappa = 0$ |
| $\varepsilon\ [m^2/s^3]$ | | $\nabla\varepsilon = 0$ |
| $\nu_t\ [m^2/s]$ | | $\nabla\nu_t = 0$ |

Table 3. Boundary conditions (with and without wall function) for the plate region.

| Parameter | plate without wall functions | plate with wall functions |
|---|---|---|
| $T\ [K]$ | $313.15\ K$ | |
| $U\ [m/s]$ | $\|U\| = 0$ | |
| $p\ [m^2/s^2]$ | calculated | |
| $p\_rgh$ $[m^2/s^2]$ | fixedFluxPressure | |
| $\alpha_t\ [m^2/s]$ | alphatJayatillekeWallFunction | |
| $\kappa\ [m^2/s^2]$ | $\kappa = 0$ | kqRWallFunction |
| $\varepsilon\ [m^2/s^3]$ | $\nabla\varepsilon = 0$ | epsilonWallFunction |
| $\nu_t\ [m^2/s]$ | $\nabla\nu_t = 0$ | nutkWallFunction |

The *inletOutlet* condition for $T$ defines: a) $\nabla T = 0$ for output regions and b) $T = T_\infty$ for input regions.

The *pressureInletOutletVelocity* condition for $U$ establishes: a) $\nabla U = 0$ for output regions and b) calculation of normal components of $U$ from $p\_rgh$ for input regions.

The *calculated* condition establishes the definition of the parameter $p$ from $p\_rgh$.

For the $p\_rgh$ field, there are two boundary conditions: *totalPressure* and *fixedFluxPressure*. The first establishes a total pressure condition $(p_0)$ for incompressible flows: $p = p_0 - 0.5|U|^2$. The second condition sets the $\nabla p\_rgh$ to guarantee the condition specified in $U$.

The *alphatJayatillekeWallFunction* condition for $\alpha_t$ defines Jayatilleke's thermal wall function model. Thus, according to Versteeg and Malalasekera (2007), there is:

$$T^+ = Pr_t\left(u^+ + 9.24\left[\left(\frac{Pr}{Pr_t}\right)^{\frac{3}{4}} - 1\right].\right.$$
$$\left.\left.\left\{1 + 0.28.\exp\left[-0.007.\left(\frac{Pr}{Pr_t}\right)\right]\right\}\right) \quad (8)$$

Finally, there are the boundary conditions for the inclusion of wall functions on the plate. The *kqRWallFunction* condition sets $\nabla\kappa = 0$ for high Reynolds flow, the *epsilonWallFunction* condition provides a wall restriction for $\varepsilon$, and finally, the *nutkWallFunction* condition sets $\nu_t$ from $\kappa$.

**Methodology for Formulation and Analysis of Results of Numerical Models**

Eighteen (18) simulations were performed in this work, divided into A) Mesh Analysis and Boundary Conditions Models and B) Physical Domain Determination Models.

The Mesh Analysis and Boundary Conditions Models aim to determine the best mesh configuration and boundary conditions for the studied problem situation. Figure 4 illustrates the sequence of tests performed, emphasizing that all simulations were made in a physical domain of dimensions 1.5 x 1.5 x 2.5 m; to be adjusted in the following steps of this work.

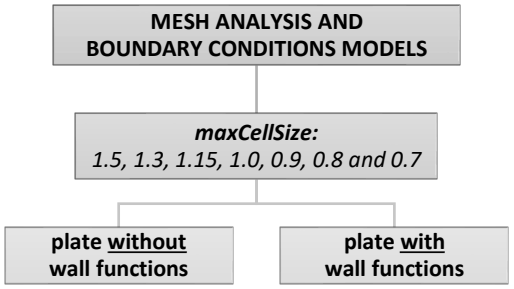


Figure 4. Test sequence of the Mesh Analysis and Boundary Conditions Models.

Then there are the Physical Domain Determination Models simulations, which were subdivided into A) Height $H_D$ Influence Study Models and B) Base Length $L_D$ Influence Study Models. Such models aim to define an optimized physical domain with less geometric influence and greater stability on the numerical results of the physical model studied, demanding less effort and computational time. All tests were performed on meshes with $maxCellSize = 0.9$ and wall functions implemented in the turbulent parameters $\kappa, \varepsilon$ and $\nu_t$ in the plate region.

The Height $H_D$ Influence Study Models have $L_D = 1.5\ m$, varying the $H_D$ parameter to 1.5, 2.5 and 3.5 m; as illustrated in Figure 5. The Base Length $L_D$ Influence Study Models have $H_D = 2.5\ m$, varying the $L_D$ parameter to 0.75, 1.5 and 3.0 m; as illustrated in Figure 6. Figure 7 schematically illustrates the sequence of tests performed on the Physical Domain Determination Models.

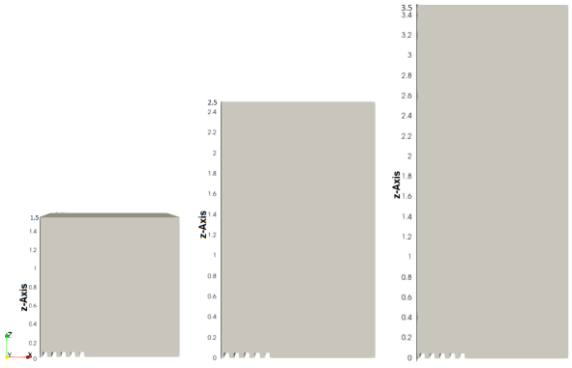

Figure 5. Height $H_D$ Influence Study Models.

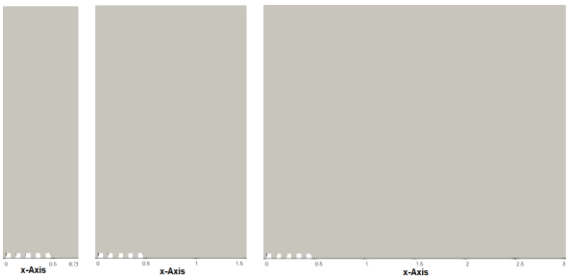


Figure 6. Base Length $L_D$ Influence Study Models.

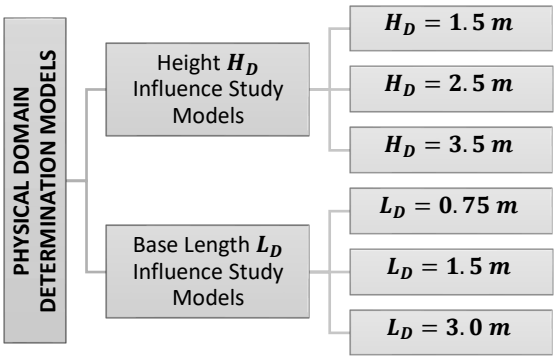


Figure 7. Test sequence of the Physical Domain Determination Models.

In all tests performed in the different models studied, there is a definition of the more suitable numerical parameters through the criteria mean absolute percentage deviation (S, calculated according to the following equation), numerical stability and simulation convergence.

$$S = \left| \frac{\overline{q''} - \overline{q''}_{REF}}{\overline{q''}_{REF}} \right| \cdot 100\% \qquad (9)$$

The average convective heat flux over the plate $(\overline{q''})$ is calculated through the utility *wallHeatFluxIncompressible* of OpenFOAM® and the term $\overline{q''}_{REF}$ relates to the results of the more refined numerical models (less *maxCellSize*) or higher geometric complexity (higher $H_D$ or $L_D$).

## RESULTS AND DISCUSSION

The analysis of the results starts with the Mesh Analysis and Boundary Conditions Models. The evolution curves of $\overline{q''}$ with the number of iterations are plotted to analyze the convergence and stability of the numerical simulations performed; according to Figure 8.

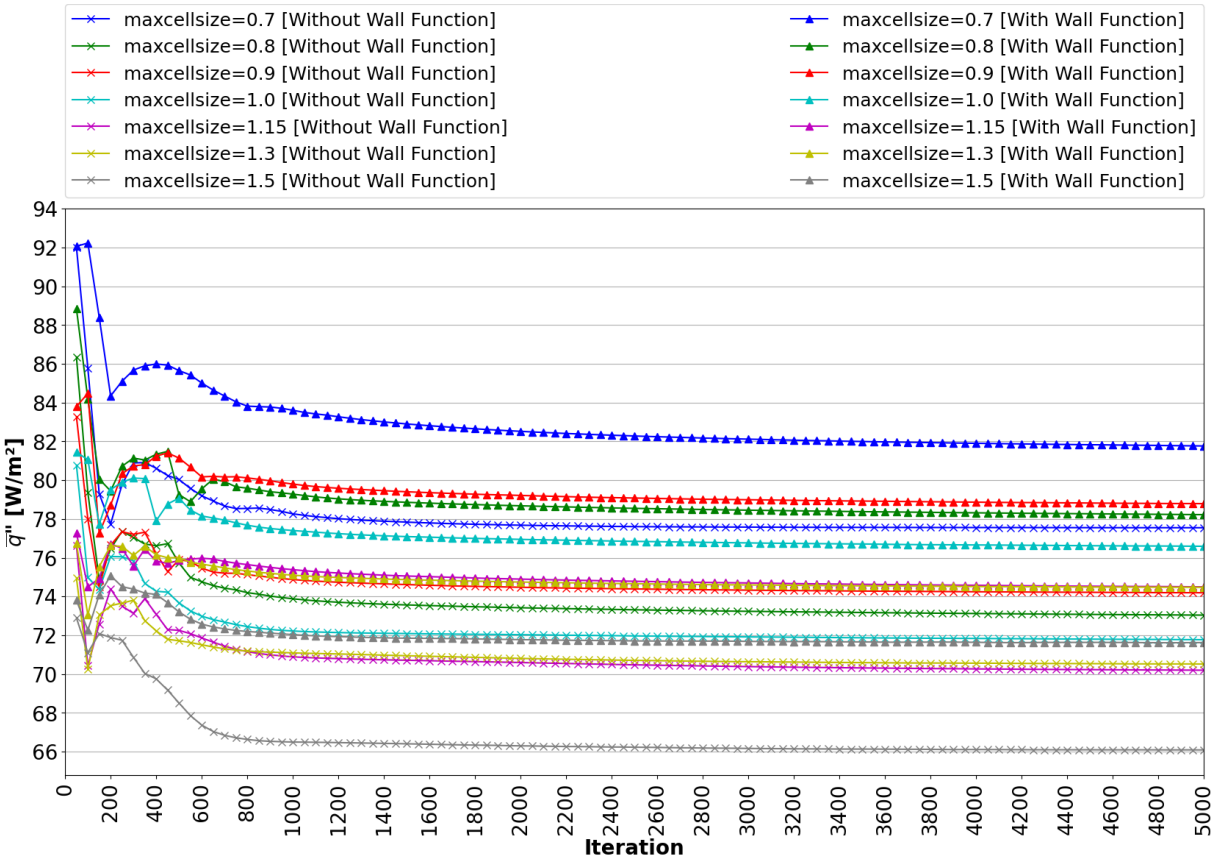


Figure 8. Results of $\overline{q''}$ versus iterations for the Mesh Analysis and Boundary Conditions Models.

From the qualitative analysis of Figure 8, it is decided to use the mesh with $maxCellSize = 0.7$ without wall functions implemented as a reference simulation for calculating $S$, according to Equation (9). This decision is based on the mesh's greater complexity (refinement level and greater number of elements) and the rapid convergence and stabilization of the solution to the steady-state.

The mesh with $maxCellSize = 0.7$ with implemented wall functions was not used as reference mesh due to the greater difficulty and iterations required to obtain a steady-state solution. This is because, despite having the same degree of topological refinement as the mesh selected as a reference, it has a more time-consuming solution convergence process; not solving steady-state even after 5000 iterations performed.

Table 4 quantitatively presents the results of $\overline{q''}$ and $S$ for the different meshes studied, after solution convergence or at the end of the iterations performed. Figure 9 shows the $S$ as a function of the $maxCellSize$ parameter for the different meshes, and boundary conditions studied.

Table 4. Quantitative results of the Mesh Analysis and Boundary Conditions Models.

| $maxCellSize$ | plate without wall functions | | plate with wall functions | |
|---|---|---|---|---|
| | $\overline{q''}$ [W/m²] | S [%] | $\overline{q''}$ [W/m²] | S [%] |
| 1.50 | 66.1061 | 14.79 | 71.6324 | 7.66 |
| 1.30 | 70.536 | 9.08 | 74.4915 | 3.98 |
| 1.15 | 70.2289 | 9.47 | 74.5344 | 3.92 |
| 1.00 | 71.8029 | 7.44 | 76.6227 | 1.23 |
| 0.90 | 74.2171 | 4.33 | 78.8228 | 1.61 |
| 0.80 | 73.1013 | 5.77 | 78.2667 | 0.89 |
| 0.70 | 77.5774 | 0.00 | 81.8296 | 5.48 |

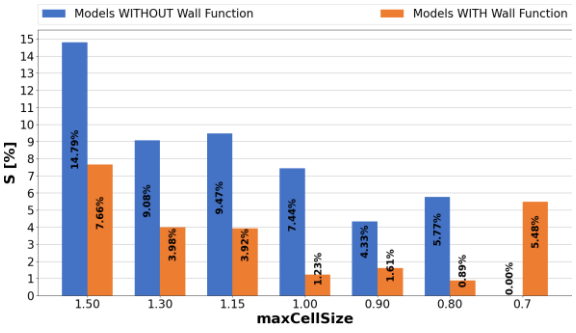


Figure 9. Results of $S$ versus $maxCellSize$ for the Mesh Analysis and Boundary Conditions Models.

From the analysis of the results, it is possible to see, compared to the simulation treated as a reference, that the use of wall functions favors obtaining solutions with greater accuracy, faster convergence, and a lesser degree of mesh refinement required. What provides advantages in terms of cost-benefit of accuracy, computational effort, and simulation time demanded.

The previous conclusion differs a little from the results observed for flat plates by Verdério Júnior *et al.* (2021a) and Verdério Júnior *et al.* (2021b) – who did not present significant differences in the numerical results between the configurations without and with wall functions. However, this conclusion is physically consistent and expresses the difficulty of formulating generalizing hypotheses about the use or not of wall functions in different geometries without further studies and analysis; at the risk of incurring unfounded conclusions.

Therefore, considering the geometric and physical differences in the solution in the study of flat and corrugated plates, the advantages of using wall functions in corrugated plates have been demonstrated.

It can be concluded, in comparison to the simulation treated as reference, that the best mesh options, in decreasing order of deviation, are: $maxCellSize = 0.7$ without wall functions, $maxCellSize = 0.8$ with wall functions ($S = 0.89\%$), $maxCellSize = 1.0$ with wall functions ($S = 1.23\%$), and $maxCellSize = 0.9$ with wall functions ($S = 1.61\%$). Emphasizing that the mesh with $maxCellSize = 0.7$ with wall functions ($S = 5.48\%$) was discarded due to the greater difficulty and time demanded in obtaining the solution in steady-state, higher order of deviation, and higher computational cost demanded. The other meshes proved to be unfeasible because presenting greater deviations and did not offer significant advantages about cost-benefit in terms of accuracy and simulation time demands.

Thus, considering the search for meshes that simultaneously combine: a) lower number of elements and lower complexity (higher $maxCellSize$), b) solution stability and fast convergence to the steady-state, and c) good accuracy; there is a decision to use the mesh with $maxCellSize = 0.9$ with wall functions implemented in the turbulent parameters $\kappa$, $\varepsilon$ and $\nu_t$.

The decision not to use the mesh with $maxCellSize = 1.0$ with wall functions is justified by its limitation of geometric construction in more complex waves (as in trapezoidal and triangular geometries), which in the presence of elements with a larger dimension (larger $maxCellSize$) tend to cause three-dimensional geometric distortions in the mesh. In turn, the mesh with $maxCellSize = 0.8$ with wall functions, compared to the chosen one, presents a deviation difference of 0.72% and 351334 additional elements; which makes its choice unfeasible, considering the small advantage of accuracy obtained at the very high increase in the computational cost demanded.

Continuing with the analysis of results, there are the Physical Domain Determination Models. The results of the Height $H_D$ Influence Study Models are shown in Table 5 and Figure 10. The simulation with

$H_D = 3.5\ m$ was admitted as the reference for the calculation of $S$, given its greater geometric complexity.

Table 5. Quantitative results of the Height $H_D$ Influence Study Models.

| $H_D\ [m]$ | Elements | $\overline{q''}$ [W/m²] | S [%] |
|---|---|---|---|
| 1.5 | 856735 | 78.4421 | 0.49 |
| 2.5 | 917535 | 78.8228 | 0.98 |
| 3.5 | 932271 | 78.0576 | 0.00 |


Figure 10. Results of $\overline{q''}$ versus iterations for the Height $H_D$ Influence Study Models.

The analysis of results in Table 5 and Figure 10 attest that the three physical models are equivalent. This conclusion is based on the numerical solution characteristics of convergence to the steady-state, stability, and very low percentage deviation between the results of the simulations performed (of the maximum order of 0.98% for the model $H_D = 2.5\ m$).

The physical characteristics of natural convection and the mechanisms of thermal plume formation demonstrate the importance of correctly determining the physical domain computational height in the mechanisms of mass and energy transport in the vertical direction (z-axis) of the studied geometry. Therefore, selecting a physical model with insufficient height could jeopardize the capture and adequate physical description of these phenomena.

From the arguments and discussions presented, it was decided to use the mesh with $H_D = 2.5\ m$. This decision is based on the characteristics of convergence and numerical stability of the solutions obtained and cost-benefit criteria about the computational effort and simulation time demanded. It is also based on the physical characteristics of the natural convection problem, and the need for a sufficient physical domain computational height not to impair the correct description of the mass and energy transport mechanisms in the direction of the gravitational axis.

Finally, there is the analysis of the Base Length $L_D$ Influence Study Models; presented in Table 6 and Figure 11. Because of the greater geometric complexity, it was decided to use the simulation with $L_D = 3.0\ m$ as a reference for the calculation of $S$.

Table 6. Quantitative results of the Base Length $L_D$ Influence Study Models.

| $L_D\ [m]$ | Elements | $\overline{q''}$ [W/m²] | S [%] |
|---|---|---|---|
| 0.75 | 763940 | 80,2506 | 0.02 |
| 1.50 | 917535 | 78,8228 | 1.80 |
| 3.00 | 906644 | 80,2657 | 0.00 |

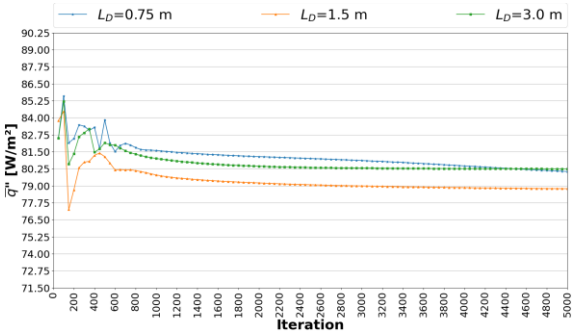


Figure 11. Results of $\overline{q''}$ versus iterations for the Base Length $L_D$ Influence Study Models.

From the analysis of Figure 11, it is observable that the simulation with $L_D = 0.75\ m$, in the interval of 5000 iterations performed, has not yet reached the convergence to the steady-state or approached this condition only at the end of the simulation. Such delay or difficulty in obtaining a solution in steady-state may be related to the reduced physical domain base size, difficulting the mass and energy transport mechanisms in the analyzed geometry and requiring more iterations for stabilization and numerical convergence of the solution. However, compared to the reference simulation, this solution presents good accuracy of results with $S = 0.02\%$, in addition to an excellent computational cost-benefit about the effort and simulation time demanded; especially considering the lower complexity and the reduced number of mesh elements.

The mesh with $L_D = 1.5\ m$ did not demonstrate cost-benefit viability, despite achieving faster convergence to the steady-state and presenting a reasonable accuracy (with $S = 1.80\%$). The same conclusion of infeasibility is also applied to the mesh with $L_D = 3.0\ m$. Observing that the two meshes, in terms of the number of elements, are practically identical – which can be understood through the characteristics and refinement boxes used in the mesh construction process. This conclusion of the infeasibility of these physical models is based on the greater amount of elements present, smaller or negligible gains in accuracy, and the higher computational cost demanded.

From all discussions, the mesh with $L_D = 0.75\ m$ proved to be the most viable option in terms of cost-effectiveness of accuracy and computational cost. This decision is based, in comparison with the more geometrically complex mesh with $L_D = 3.0\ m$,

on the high accuracy (with a very low deviation) and lower topological complexity (comparative reduction of 142704 elements); despite the greater difficulty and the greater number of iterations required to obtain a steady-state solution.

## CONCLUSIONS

The present case study analyzed the best physical-numerical formulation for the modeling and studying natural convection heat transfer over isothermal plates with square waves and under conditions of high Rayleigh number. Numerical parameters related to the mesh refinement level, boundary conditions and physical domain geometry were widely discussed, selecting those that best fit the studied problem.

The Mesh Analysis and Boundary Conditions Models demonstrated advantages in using wall functions as boundary conditions for $\kappa$, $\varepsilon$ and $\nu_t$ in the plate region. Obtaining greater accuracy, faster convergence to the steady-state, lower mesh refinement required, and less computational effort and time demanded in the simulations performed. Such results and conclusions complement the studies by Verdério Júnior *et al.* (2021a) and Verdério Júnior *et al.* (2021b).

In terms of cost-effectiveness, the mesh with $maxCellSize = 0.9$ with wall functions implemented in $\kappa$, $\varepsilon$ and $\nu_t$ for the plate region proved to be more suitable for the studied problem.

The Physical Domain Determination Models – observing the criteria of accuracy, computational effort and time demanded, numerical stability and solution convergence – proved to be more viable to use a computational domain of double symmetry with dimensions $(L_D \times L_D \times H_D)$ $0.75 \times 0.75 \times 2.5$ m.

Finally, the numerical analysis methodology used (exclusively with free and open-source software) demonstrates alternatives to researching conditions of greater budget restriction and lack of investment in R&D; a condition that seems to have intensified in the current scenario of the COVID-19 pandemic and that affects industries, universities and the most diverse areas of knowledge.

## ACKNOWLEDGEMENTS

The authors thank the Instituto Federal de Educação, Ciência e Tecnologia de São Paulo (IFSP), Araraquara campus, the Universidade Estadual Paulista "Júlio de Mesquita Filho" (UNESP), Faculdade de Engenharia (FEB), Bauru campus, and Instituto Superior Técnico (IST), Universidade de Lisboa for providing the workforce and the conditions to produce this research project.

## REFERENCES

Bejan, A., 2013, Convection Heat Transfer, John wiley & Sons.

Bird, R. B., Stewart, W. E. and Lightfoot, E. N., 2004, Transport Phenomena, John Wiley & Sons.

Çengel, Y. A., and Cimbala, J. M., 2015, Mecânica dos Fluidos: Fundamentos e Aplicações, AMGH (in Portuguese).

Çengel, Y. A., and Ghajar, A. J., 2012, Transferência de Calor e Massa: Uma abordagem prática, AMGH (in Portuguese).

Fox, R. W. et al., 2018, Introdução à Mecânica dos Fluidos, LTC (in Portuguese).

Fishenden, M., and Saunders, O., 1965, An Introduction to Heat Transfer, Clarendon Press, Oxford.

Gonçalves, D. M., Sanchez, L. E. A., and Verdério Júnior, S. A., 2021, Correlation between Leidenfrost Temperature, Cooling Capacity snd Machining Temperature: An Experimental Study of Cutting Fluids, Revista de Engenharia Térmica, Vol. 20, No. 3, p. 10-15. DOI: http://dx.doi.org/10.5380/reterm.v20i3.83264.

Incropera, F. et al., 2008, Fundamentos da Transferência de Calor e de Massa, LTC (in Portuguese).

Juretic, F., 2015, User Guide cfMesh v1.1. Creative Fields, Zagreb, Croatia, 2015. URL: http://cfmesh.com/wp-content/uploads/2015/09/User_Guide-cfMesh_v1.1.pdf. Retrieved 04 Mar. 2022.

Kitamura, K., Mitsuishi, A., Suzuki, T. and Kimura, F., 2015, Fluid Flow and Heat Transfer of Natural Convection Adjacent to Upward-Facing, Rectangular Plates of Arbitrary Aspect Ratios, International Journal of Heat and Mass Transfer, Vol. 89, pp. 320–332.

Menter, F., Kuntz, M. and Langtry, R., 2003, Ten Years of Industrial Experience With the SST Turbulence Model, in: International Symposium on Turbulence: Heat and Mass Transfer, Begell House, Antalya, pp. 625-632.

Moukalled, F., Mangani, L. and Darwish, M., 2015, The Finite Volume Method in Computational Fluid Dynamics: An Advanced Introduction with OpenFOAM® and Matlab®, Springer.

OpenCFD, 2020, OpenFOAM: The Open Source CFD Toolbox, User Guide (v2012), OpenCFD Ltd.

Pope, S. B., 2000, Turbulent Flows, England: Cambridge University Press.

Silva, V. R. et al., 2021, Study and Validation of meshes in turbulent isothermal problems of natural convection in flat plates, Revista de Engenharia Térmica, Vol. 20, No. 2, p. 33-40. DOI: http://dx.doi.org/10.5380/reterm.v20i2.81785.

Verdério Júnior, S. A., Aplicação de um modelo numérico na otimização de fornos alimentícios usando o OpenFOAM®, 2015, Thesis (Master's degree) – Universidade Estadual Paulista Júlio de Mesquita Filho, Faculdade de Engenharia, Bauru,

Master's degree in mechanical engineering, 173 p (in Portuguese).

Verdério Júnior, S. A. et al., 2021a, Physical–numerical parameters in turbulent simulations of natural convection on three-dimensional square plates, International Journal of Numerical Methods for Heat & Fluid Flow, Vol. 3, No 2, p. 761–784. DOI: https://doi.org/10.1108/HFF-02-2021-0128.

Verdério Júnior, S. A., Scalon, V. L., and Oliveira, S. R., 2021b, Physical–numerical parameters in laminar simulations of natural convection on three-dimensional square plates, International Journal of Numerical Methods for Heat & Fluid Flow. DOI: https://doi.org/10.1108/HFF-07-2021-0478.

Verdério Júnior, S. A. et al., 2021c, Dimensionless Physical-Mathematical Modeling of Turbulent Natural Convection, Revista de Engenharia Térmica, Vol. 20, No. 3, p. 37-43. DOI: http://dx.doi.org/10.5380/reterm.v20i3.83269.

Verdério Júnior, S. A. et al., 2021d, Experimental Methodology for the Study of Natural Convection on Flat and Corrugated Plates, Revista de Engenharia Térmica, Vol. 20, No. 4, p. 37-43. DOI: http://dx.doi.org/10.5380/reterm.v20i3.83269.

Versteeg, H. K. and Malalasekera, W., 2007, An Introduction to Computational Fluid Dynamics – The Finite Volume Method, Longman Scientific and Technical.

Vieser, W., Esch, T., and Menter, F., 2002, Heat transfer predictions using advanced two-equation turbulence models, CFX Validation Report.